Eur. Phys. J. D **32**, 391–396 (2005)
DOI: 10.1140/epjd/e2004-00190-3

THE EUROPEAN PHYSICAL JOURNAL D

Time-resolved homodyne characterization of individual quadrature-entangled pulses

J. Wenger, A. Ourjoumtsev, R. Tualle-Brouri, and P. Grangier[a]

Laboratoire Charles Fabry de l'Institut d'Optique, CNRS UMR 8501, 91403 Orsay, France

Received 29 September 2004
Published online 21 December 2004 –

Abstract. We describe a simple and efficient set-up to generate and characterize femtosecond quadrature-entangled pulses. Quantum correlations equivalent to about 2.5 dB squeezing are efficiently and easily reached using the non-degenerate parametric amplification of femtosecond pulses through a single-pass in a thin (100 μm) potassium niobate crystal. The entangled pulses are then individually sampled to characterize the non-separability and the entropy of formation of the states. The complete experiment is analysed in the time-domain, from the pulsed source of quadrature entanglement to the time-resolved homodyne detection. This particularity allows for applications in quantum communication protocols using continuous-variable entanglement.

PACS. 42.50.Dv Nonclassical states of the electromagnetic field, including entangled photon states; quantum state engineering and measurements – 03.67.-a Quantum information – 03.65.Wj State reconstruction, quantum tomography

1 Introduction

Quantum correlations have properties which cannot be reproduced by the rules of classical physics [1,2]. More specifically, quantum entanglement is now acknowledged as a physical resource, which is needed to perform new quantum information processing tasks, such as quantum teleportation, dense coding, quantum cryptography or quantum computation [3]. To perform these protocols, quantum continuous variables [4] have recently emerged as a relevant alternative to discrete-levels systems. This is particularly true in the optical domain, where entanglement of quantum continuous variables provides a tool of major importance for developing new quantum communication devices, based on homodyne detection of intense beams, rather than photon-counting detectors.

In order to characterize simply quantum communication protocols, it is very convenient to consider them as the exchange of some symbols, which carry the relevant information and can be accessed individually. Hence, an important issue for quantum communication is to develop communication schemes operating in a pulsed regime, that are able to manipulate individually each quantum state involved in the exchange. The analysis of such protocols is then very easy in terms of information transfers [5,6]. However, since the landmark experiment by Ou et al. [7,8], most of the experiments relying on entangled quantum continuous variables have been performed by using continuous wave (rather than pulsed) entangled light beams [9–18]. In addition, the characterization of the quantum correlations was performed in the spectral domain (i.e. by using radio-frequency spectrum analysers), rather than in the time domain. As a consequence, even if they are actually pulsed [19,20], such experiments cannot be easily used to implement quantum communication protocols, because they do not provide access to each individual entangled pulse. These difficulties might be solved by developing a quantum theory of analog modulation, evaluating the information transfer by defining appropriate time-bandwidth limited modes, and quantizing them. But as long as no such theory has been proposed, addressing well-separated "symbols" — each associated to one quantum state — clearly appears to be much easier, both from a practical and a fundamental point of view.

In this article, we present a new scheme for the generation of quadrature-entangled light pulses, which can be individually accessed and characterized. This experiment is based on the non-degenerate parametric amplification of ultrafast (150 fs) pulses through a single pass in a thin potassium niobate ($KNbO_3$) crystal. Thanks to the high peak power of the femtosecond pulses and the high nonlinear coefficient of the $KNbO_3$ crystal, significant quantum correlations (equivalent to about 2.5 dB squeezing) have been reached. The non-separability of the entangled pulses is then directly characterized by a time-resolved homodyne detection, which samples the quantum properties of each individual incoming pulse.

Recently, our team has developed a similar set-up which operated in a degenerate configuration to produce pulsed squeezed states [21]. The experiment described here presents some further developments of this scheme

[a] e-mail: philippe.grangier@iota.u-psud.fr

towards pulsed quadrature entanglement. As said above, all our set-up operates in the pulsed regime, from the source of entanglement to the time-resolved detection, so our analysis is completely carried out in the time domain, and not in the frequency domain. Since the quadrature-entangled pulses are efficiently and easily generated through a single pass in a nonlinear crystal using non-degenerate parametric optical amplification (NOPA), the set-up provides a simple and compact source for pulsed quadrature entanglement.

This paper is organized as follows: first, we review some general results concerning the manipulation and the characterization of quadrature-entanglement (Sect. 2). Then the experimental set-up is described in details (Sect. 3) before presenting the results of our pulsed homodyne measurements (Sect. 4).

2 Quadrature entanglement: principles and characterization

2.1 Producing entanglement: the non-degenerate parametric amplifier

A well-known way to generate a two-mode state whose quadrature components are entangled is to use an optical parametric amplifier in a non-degenerate configuration [22,23]. Let us denote by (X, P) the quadrature components of one mode of the light field. These quantum operators follow the commutation relation $[X, P] = 2iN_0$ and thus the Heisenberg uncertainty $\Delta^2 X\, \Delta^2 P \geq {N_0}^2$, where $\Delta^2(.)$ denotes the variance of the observable (N_0 is a scaling constant, which equals to the standard shot noise variance). The quadrature components (X_A, P_A) and (X_B, P_B) of the output modes ("signal" and "idler") of a perfect non-degenerate parametric amplifier are given by [22,23]:

$$\begin{aligned} X_A &= \cosh r\, X_{A,in} + \sinh r\, X_{B,in} \\ P_A &= \cosh r\, P_{A,in} - \sinh r\, P_{B,in} \\ X_B &= \cosh r\, X_{B,in} + \sinh r\, X_{A,in} \\ P_B &= \cosh r\, P_{B,in} - \sinh r\, P_{A,in} \end{aligned} \quad (1)$$

where $(X_{A,in}, P_{A,in})$ and $(X_{B,in}, P_{B,in})$ stand for the input modes and r is the squeezing factor, which depends on the strength of the nonlinear interaction. In the following, we will consider the case where the input modes are in the vacuum state. The state generated by NOPA is then generally called *two-mode squeezed state*, as it bears some quantum correlations between the quadratures:

$$\langle X_A\, X_B \rangle = -\langle P_A\, P_B \rangle = \sinh 2r\, N_0 \quad (2)$$

$$\langle (X_A - X_B)^2 \rangle = \langle (P_A + P_B)^2 \rangle = 2\, e^{-2r}\, N_0. \quad (3)$$

In the case of infinite nonlinear effects, $r \to \infty$, the quantum correlations between the quadratures would become perfect (e.g. $\langle (X_A - X_B)^2 \rangle \to 0$). This case corresponds to the famous Einstein, Podolsky and Rosen (EPR) Gedanken-experiment proposed in 1935 [1].

2.2 Characterizing entanglement: the non-separability criterion

For a given state composed of two modes A and B, a relevant question is to determine whether this state carries some entanglement or not. For quantum continuous variables, Duan et al. [24] and Simon [25] have independently formulated a sufficient condition for a state to be non-separable:

$$\mathcal{I}_{\rm DS} = \frac{1}{2}\left[\Delta^2(X_A - X_B) + \Delta^2(P_A + P_B)\right] < 2\, N_0. \quad (4)$$

Dealing with a symmetrical Gaussian two-mode state, such as the one generated by NOPA, this condition turns out to be a necessary and sufficient condition of non-separability. In relation with the EPR situation quoted above, another criterion often used to quantify the quantum correlations between the entangled modes is the "Reid-EPR" criterion [22], which applies to the products of the conditional variances: $V_{X_B|X_A}\, V_{P_B|P_A} < {N_0}^2$. Quantum states that are non-classical according to the Reid-EPR criterion will automatically be non-separable according to the Duan-Simon condition (4), but the reverse is not true. Though the Duan-Simon criterion appears less relevant with respect to the EPR situation, we will use it in the present work, because it is quite appropriate as a threshold for the possibility of entanglement distillation, which is a central goal for quantum communications.

In the case of the state generated by perfect NOPA, one gets $\mathcal{I}_{\rm DS} = 2\, e^{-2r}\, N_0$. Thus the violation of the Duan-Simon condition for separability occurs as soon as $r > 0$ and increases with the strength r of the nonlinear interaction. This suggests to use $\mathcal{I}_{\rm DS}$ to quantify the entanglement. However, a relevant measure of entanglement has to satisfy some constraints given in [26,27]. Unfortunately, $\mathcal{I}_{\rm DS}$ does not fulfil these constraints and thus does not provide a "true" measure of entanglement. Nevertheless, $\mathcal{I}_{\rm DS}$ is a direct witness of non-separability and can be used to compute a relevant measure of entanglement for Gaussian states, as we will see now.

2.3 Quantifying entanglement: the entropy of formation

For a bipartite pure state, the amount of entanglement is uniquely defined by the Von Neumann entropy of one of the sub-state [27]. However, for a mixed state, the definition of the quantity of entanglement is not unique, and has led to different theoretical proposals. Among them, let us pay some attention to the entropy of formation, introduced by Wooters in [28]. This quantity represents the number of maximally entangled pairs of qubits necessary to prepare the observed correlations, and it has been explicitly calculated in the case of Gaussian states by Giedke and coworkers [29]. For a symmetric two-mode

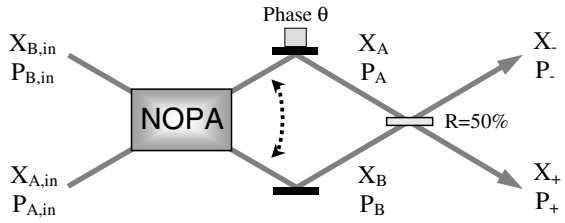

Fig. 1. Simplified scheme of the experimental set-up used to characterize the quadrature entanglement produced during single-pass non-degenerate parametric amplification (NOPA). The beam (X_+, P_+) is then measured by a time-resolved homodyne detection.

Gaussian state whose covariance matrix reads

$$\gamma = \begin{pmatrix} V & 0 & K_x & 0 \\ 0 & V & 0 & -K_p \\ K_x & 0 & V & 0 \\ 0 & -K_p & 0 & V \end{pmatrix} \tag{5}$$

the entropy of formation is then given by the formula:

$$E_{\mathrm{F}} = f\left(\sqrt{(V-K_x)(V-K_p)}\right) \tag{6}$$

with $f(x) = c_+(x)\log_2 c_+(x) - c_-(x)\log_2 c_-(x)$ and $c_\pm(x) = [x^{-1/2} \pm x^{1/2}]^2/4$. Consequently, for a state generated by NOPA, the entropy of formation is directly linked to the Duan-Simon quantity $\mathcal{I}_{\mathrm{DS}}$ as noticed in [18]:

$$E_{\mathrm{F}} = f\left(\frac{\mathcal{I}_{\mathrm{DS}}}{2\,N_0}\right). \tag{7}$$

2.4 Simple experimental measurements of quadrature entanglement

The method experimentally developed here to characterize the Gaussian quadrature-entangled states is largely inspired from these theoretical results and aims at directly measuring the Duan-Simon quantity $\mathcal{I}_{\mathrm{DS}}$. The principle of our scheme is depicted in Figure 1. The two entangled modes generated by NOPA are mixed on a beamsplitter of $R = 50\%$ reflectivity, while one output mode of the beamsplitter is sent to a time-resolved homodyne detection for pulse-sensitive quadrature measurements.

Let θ denote the relative phase between the entangled pulses. When the two entangled modes A, B are mixed in phase on the beamsplitter, $\theta = 0$, the output mode of the beamsplitter (X_+, P_+) reads:

$$\begin{aligned} X_+ &= \frac{1}{\sqrt{2}}(X_A + X_B) = \frac{e^r}{\sqrt{2}}(X_{A,in} + X_{B,in}) \\ P_+ &= \frac{1}{\sqrt{2}}(P_A + P_B) = \frac{e^{-r}}{\sqrt{2}}(P_{A,in} + P_{B,in}). \end{aligned} \tag{8}$$

Thus the state at the output of the beamsplitter is a squeezed state, and the corresponding variances in quadratures are either above or below the shot noise level: $\Delta^2 X_+ = e^{2r}N_0$, $\Delta^2 P_+ = e^{-2r}N_0$. Measuring $\Delta^2 P_+ = \Delta^2(P_A + P_B)/2$ with the homodyne detection gives directly one term to be used in the Duan-Simon quantity $\mathcal{I}_{\mathrm{DS}}$ (4).

If a relative phase of $\theta = \pi$ is set between the two entangled modes A, B, the output mode of the beamsplitter (X_+, P_+) then reads:

$$\begin{aligned} X_+ &= \frac{1}{\sqrt{2}}(X_A - X_B) = \frac{e^{-r}}{\sqrt{2}}(X_{A,in} - X_{B,in}) \\ P_+ &= \frac{1}{\sqrt{2}}(P_A - P_B) = \frac{e^{r}}{\sqrt{2}}(P_{A,in} - P_{B,in}). \end{aligned} \tag{9}$$

This is still a squeezed state, but the squeezed quadrature has now turned to the X quadrature. Measuring $\Delta^2 X_+ = \Delta^2(X_A - X_B)/2$ with the homodyne detection, one gets directly the other term of the Duan-Simon quantity $\mathcal{I}_{\mathrm{DS}}$. Thus by mixing the entangled pulses on a beamsplitter and controlling the relative phase θ between them and between the local oscillator used in the homodyne detection, one can measure all the relevant parameters to express the Duan-Simon quantity $\mathcal{I}_{\mathrm{DS}}$. More generally, one can easily show that for any phase θ the quadrature $\sin(\theta/2)\,X_+ + \cos(\theta/2)\,P_+$ is squeezed while the quadrature $\cos(\theta/2)\,X_+ - \sin(\theta/2)\,P_+$ is anti-squeezed. Thus dephasing the EPR beams by θ before the recombination makes the phase-space uncertainty ellipse turn by an angle of $\theta/2$, but it keeps the ellipticity constant.

One interesting feature of this characterization method is that it provides simply the necessary quantity $\mathcal{I}_{\mathrm{DS}}$ to check for the non-separability from equation (4) and to quantify the entanglement from equation (7). Only one homodyne detection set-up is needed, which greatly simplifies the experiment. This method appears also quite similar to the set-ups used for dense coding experiments [10,30,31]. Let us now turn to the physical implementation of these principles in the pulsed regime.

3 Experimental set-up

We have recently developed a new scheme for pulsed squeezed light generation [21]. This experiment is based on the degenerate parametric amplification of femtosecond pulses. Here we extend this experiment and pass to the non-degenerate regime of parametric amplification.

The experimental scheme is presented in Figure 2. The initial pulses are obtained from a cavity-dumped titanium-sapphire laser (Tiger-CD, Time-Bandwidth Products), delivering nearly Fourier-transform limited pulses at 846 nm, with a duration of 150 fs, an energy of 40 nJ, and a pulse repetition rate of 780 kHz. These pulses are frequency doubled in a single pass through a thin (100 μm) crystal of potassium niobate ($KNbO_3$). This crystal is set inside a small vacuum chamber and peltier-cooled down to about -14 °C to obtain non-critical (90 degrees) type-I phase-matching for second harmonic generation (SHG) at 846 nm. The choice for a thin crystal length allows for

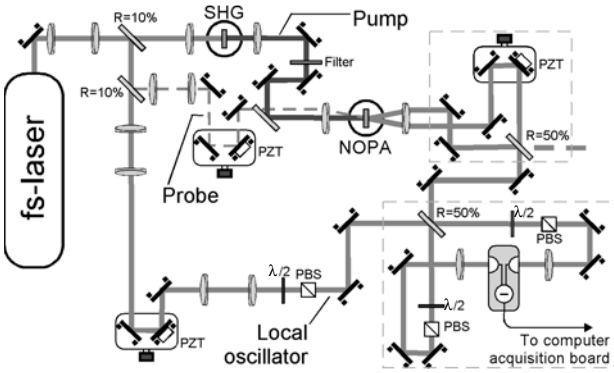

Fig. 2. Experimental set-up. SHG second harmonic generation; NOPA non-degenerate parametric amplification; PZT piezoelectric transducer; PBS polarizing beamsplitter.

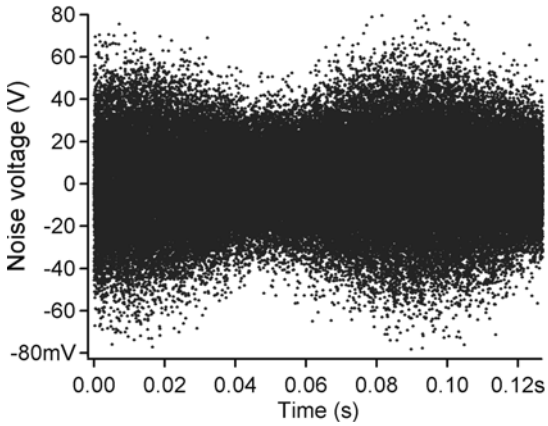

Fig. 3. Recorded noise pulses while linearly scanning the LO phase, when the entangled beams are mixed in phase ($\theta = 0$) at the 50−50 beamsplitter. Each dot corresponds to the measurement of one incoming pulse.

a wide phase-matching bandwidth and avoids the conditions of large group-velocity mismatch, contrary to the previously reported use of thick $KNbO_3$ crystals [32,33]. Even for the short interaction length used here, $KNbO_3$ proved to be suitable to our applications thanks to its high non linear coefficient (about 12 pm/V) and non-critical phase-matching. Typically, the SHG efficiency obtained is about 28% (corrected from losses).

A small fraction (1%) of the fundamental beam is taken out to serve as a probe to study classical parametric amplification occurring in a similar $KNbO_3$ crystal used in a single-pass type-I spectrally degenerate but spatially non-degenerate configuration. This spatial non-degeneracy is obtained by shifting horizontally the probe beam before focusing inside the crystal. Thanks to the focusing lens, this shift is transformed into an angular difference between the propagation directions of the pump and the probe beam within the crystal (see Fig. 2). For small angular differences of about 3° within the crystal, the phase-matching condition can still be fulfilled by lowering the temperature of the crystal by a few degrees. The average power of the probe beam after the nonlinear interaction is directly measured by a standard silicon photodiode, which allows to estimate the parametric gain. For a well-chosen angular shift so that the probe and the pump wave vectors do not overlap, the parametric gain does not depend of the relative phase between the pump and the probe beam. This condition indicates that the non-degenerate configuration is strictly reached over the whole spatial extend of the beams [23,34]. We have experimentally optimised the overlap between the pump and the probe beam to maximise the amplification gain. For the best configuration, the probe waist was set to be about $\sqrt{2}$ times smaller than the pump waist inside the crystal. Then, the best amplification obtained was 1.24. This gain was checked to be independent of the probe phase and average power.

The two beams ("signal" and "idler") resulting from the classical parametric amplification of the probe are mixed on a beamsplitter of $R = 50\%$ reflectivity, in order to implement the entanglement characterization method described in Section 2.4. One output mode of the beamsplitter is then sent to the balanced homodyne detection, and interferes with the local oscillator beam (LO). The homodyne detection is set to be directly sensitive to the incoming pulse distribution in the time domain. For each pulse, the fast acquisition board (National Instruments PCI-6111E) samples one value of the signal quadrature in phase with the local oscillator [6,35,36]. The data presented below is obtained directly from these individual pulse measurements. Pulsed homodyning is technically more challenging than frequency-resolved homodyning because low-frequency noises cannot be filtered out. Each arm of the detection has to be carefully balanced (with a typical rejection better than 10^{-4}) even for ultra-low frequency noises. By blocking the squeezed beam, the detection was checked to be shot-noise limited in the time domain, showing a linear dependence between LO power and the noise variance up to 2.5×10^8 photons per pulse. This corresponds to an average LO power of 45 μW, at a repetition rate of 780 kHz and in the femtosecond regime. The electronic noise was low enough to ensure a ratio larger than 11 dB between shot noise and electronic noise variances.

4 Pulsed homodyne measurements

4.1 Characterization of the non-separability criterion

The probe beam being blocked, the amplifier operates in a pulsed parametric down-conversion regime to generate a two-mode squeezed state. A first piezo-electric transducer allows to finely control the relative phase θ between the two entangled pulses before the recombination beamsplitter. A second piezo transducer is also used to control the relative phase of the local oscillator, which commands the quadrature component measured by the homodyne detection. Figure 3 displays the recorded noise pulses while scanning the local oscillator phase, when the quadrature-entangled beams are mixed in phase, $\theta = 0$. Figure 4 presents the corresponding quadrature variance, when the

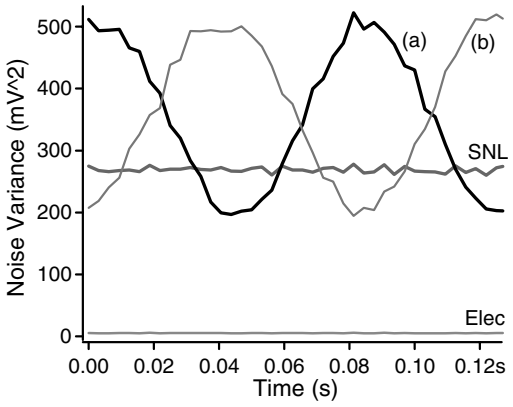

Fig. 4. Quadrature noise variance of the recombined beam (X_+, P_+) (plotted in a linear scale and computed over blocks of 2500 samples) while linearly scanning the LO phase, together with the shot noise level (SNL) and the electronic noise level. The curve (a) corresponds to the case when the entangled beams are mixed in phase ($\theta = 0$), while they are dephased by $\theta = \pi$ for the curve (b).

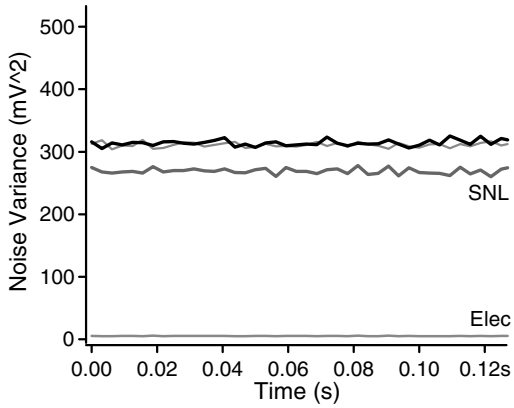

Fig. 5. Quadrature noise variance (dark curve) of one entangled beam (plotted in a linear scale and computed over blocks of 2500 samples) while linearly scanning the LO phase. The other entangled beam is blocked before the 50−50 beamsplitter. The second light gray curve above the SNL corresponds to the reverse situation by blocking the other beam.

entangled beams are in phase, $\theta = 0$ (a), or dephased by $\theta = \pi$ (b) at the 50−50 beamsplitter. As expected for the squeezed states generated by recombining the entangled pulses, the measured noise variance passes below the shot noise level (SNL) for some phase values of the local oscillator. The measured correlation variance (with no correction) is $0.70\,N_0$ (–1.55 dB below the shot noise level SNL), while the corresponding anti-squeezed variance is $1.96\,N_0$ (2.92 dB above SNL).

To characterize the entanglement of the two-mode state produced by NOPA, it appears logical to compensate for the homodyne detection efficiency. A homodyne detection with an efficiency η measures $X_{det} = \sqrt{\eta}X_+ + \sqrt{1-\eta}X_{vac}$ where X_{vac} is a vacuum mode. Therefore, the variance of the squeezed state is $\Delta X_+^2 = \left[\Delta X_{det}^2 - (1-\eta)N_0\right]/\eta$. The procedure to measure this detection efficiency is well established from squeezing experiments [21]. The overall detection efficiency is given as $\eta = \eta_T \eta_H^2 \eta_D = 68\%$, where we have independently measured the overall transmission $\eta_T = 93\%$, the mode-matching visibility $\eta_H = 88\%$ (obtained from the interference fringes between the local oscillator and a seed beam set for maximum classical amplification), and the detectors efficiency (Hamamatsu S3883) $\eta_D = 94.5\%$. Given this evaluation of the homodyne efficiency, one can evaluate the correlation variance of the pulses before the homodyne detection, which is found to be $0.56\,N_0$ (–2.52 dB below SNL).

This experiment was repeated several times for different relative phases θ between the entangled pulses before the recombination. This allowed us to check the symmetry of the state produced: we measured the same correlation variance for $\theta = 0$, $\theta = \pi$ and several other phases (within reasonable statistical errors less than $0.01\,N_0$, see Fig. 4). Consequently, we can state that the correlations between the quadratures are equal to $\Delta^2(X_A - X_B)/2 = \Delta^2(P_A + P_B)/2 = 0.56\,N_0$. The Duan-Simon quantity amounts then to $\mathcal{I}_{\rm DS} = 1.12\,N_0$, which is clearly below the threshold for separability ($2\,N_0$) given by equation (4). This results attests for the quantum entanglement (non-separability) of the pulsed state generated by NOPA. One may also quantify the entanglement available thanks to the entropy of formation given by equation (7), which provides $E_{\rm F} = 0.44$ ebit.

4.2 Characterization of the covariance matrix

Theoretically, a general Gaussian state is fully characterized by its mean values of quadratures together with its covariance matrix γ, which comprises the second moments of the conjugate quadratures X, P. For a two-mode state, the general covariance matrix γ contains 16 terms. In our case however, the two-mode squeezed state emerging from NOPA is generated and handled in a symmetric way. This point was experimentally checked as discussed in the previous subsection. Consequently, for our symmetric state, the corresponding covariance matrix can be reduced to the form given by equation (5), with $V\,N_0 = \Delta^2 X_A = \Delta^2 P_A = \Delta^2 X_B = \Delta^2 P_B$ and $K_x\,N_0 = K_p\,N_0 = \frac{1}{2}\langle X_A X_B + X_B X_A\rangle = -\frac{1}{2}\langle P_A P_B + P_B P_A\rangle$. This means that for the optimal choice of quadratures there is no cross-quadrature correlations. Let us also point out that for Gaussian states the covariance matrix can always be reduced to the form (5) using local unitary operations [24].

By blocking one entangled beam before the 50−50 beamsplitter, we have measured the diagonal terms of the covariance matrix (up to the transmission of 50% of the beamsplitter and the homodyne detection efficiency η). Our results using the time-resolved homodyne detection are displayed in Figure 5. For the two entangled beams, we have measured a variance of $1.17 \pm 0.01\,N_0$, which can be related to $V = 1.50$ before the 50−50 beamsplitter (to get this value, we have corrected for the 50% transmission of the beamsplitter and the homodyne detection efficiency

$\eta = 68\%$). The off-diagonal terms in the covariance matrix (5) can be evaluated by noticing that thanks to our squeezing measurement $\Delta^2 X_+$ we get:

$$\begin{aligned}\Delta^2 X_+ &= \frac{1}{2}\,\Delta^2(X_A - X_B) \\ &= \frac{1}{2}\,\left(\Delta^2 X_A + \Delta^2 X_B - \langle X_A X_B + X_B X_A\rangle\right) \\ &= (V - K_x)\,N_0. \end{aligned} \tag{10}$$

With $V = 1.50$ and $\Delta^2 X_+/N_0 = 0.56$, we get directly $K_x = K_p = 0.94$. Thus the reconstructed covariance matrix of the experimental entangled pulses reads:

$$\gamma = \begin{pmatrix} 1.50 & (0) & 0.94 & (0) \\ (0) & 1.50 & (0) & -0.94 \\ 0.94 & (0) & 1.50 & (0) \\ (0) & -0.94 & (0) & 1.50 \end{pmatrix}. \tag{11}$$

The values set to zero due to symmetry considerations are indicated by parenthesis. A similar procedure has already been followed by Bowen et al. [13], but in the case of continuous-wave light detected around 3.5 or 6.5 MHz using a spectrum analyser.

5 Conclusion

An efficient set-up to generate and characterize femtosecond quadrature-entangled pulses is presented, using a complete time domain analysis. Pulsed quadrature-entangled beams are efficiently generated using non-degenerate parametric amplification in a single-pass configuration. This set-up leads to correlations equivalent to about 2.5 dB squeezing, that have been recorded using a time-resolved homodyne detection. The non-separability of the states has then been characterized using the Duan-Simon criterion with $\mathcal{I}_{\rm DS} = 1.12\,N_0$ ($< 2\,N_0$), and the available entanglement has been quantified using the entropy of formation to $E_{\rm F} = 0.44$ ebit. The association of this simple and compact source for quadrature entanglement together with the time-resolved homodyne detection provides all the ressources for future quantum communication protocols using continuous variable entanglement.

This work was carried out in the framework of the European IST/FET project "COVAQIAL".

References

1. A. Einstein, B. Poldolsky, N. Rosen, Phys. Rev. **47**, 777 (1935)
2. J.S. Bell, *Speakable and Unspeakable in Quantum Mechanics* (Cambridge University Press, Cambridge, 1988)
3. M.A. Nielsen, I. Chuang, *Quantum computation and quantum information* (Cambridge University Press, Cambridge, 2000)
4. S.L. Braunstein, A.K. Pati, *Quantum Information with Continuous Variables* (Kluwer Academic, Dordrecht, 2003)
5. C.E. Shannon, Bell Syst. Tech. J. **27**, 623 (1948)
6. F. Grosshans, G. Van Assche, J. Wenger, R. Brouri, N.J. Cerf, Ph. Grangier, Nature **421**, 238 (2003)
7. Z.Y. Ou, S.F. Pereira, H.J. Kimble, K.C. Peng, Phys. Rev. Lett. **68**, 3663 (1992)
8. Z.Y. Ou, S.F. Pereira, H.J. Kimble, Appl. Phys. B **55**, 265 (1992)
9. A. Furusawa, J. Sorensen, S.L. Braunstein, C.A. Fuchs, H.J. Kimble, E. Polzik, Science **282**, 706 (1998)
10. Y. Zhang, H. Wang, X. Li, J. Jing, C. Xie, K. Peng, Phys. Rev. A **62**, 023813 (2000)
11. C. Schori, J.L. Sørensen, E.S. Polzik, Phys. Rev. A **66**, 033802 (2002)
12. W.P. Bowen, R. Schnabel, P.K. Lam, T.C. Ralph, Phys. Rev. Lett. **90**, 043601 (2004)
13. W.P. Bowen, R. Schnabel, P.K. Lam, T.C. Ralph, Phys. Rev. A **69**, 012304 (2004)
14. J. Mizuno, K. Wakui, A. Furusawa, M. Sasaki, preprint `arXiv:quant-ph/0402040` (2004)
15. L. Longchambon, J. Laurat, T. Coudreau, C. Fabre, Eur. Phys. J. D **30**, 287 (2004)
16. J. Laurat, T. Coudreau, G. Keller, N. Treps, C. Fabre, Phys. Rev. A **70**, 042315 (2004)
17. W.P. Bowen, N. Treps, R. Schnabel, P.K. Lam, Phys. Rev. Lett. **89**, 253601 (2002)
18. V. Josse, A. Dantan, A. Bramati, M. Pinard, E. Giacobino, Phys. Rev. Lett. **92**, 123601 (2004)
19. C. Silberhorn, P.K. Lam, O. Weiss, F. Konig, N. Korolkova, G. Leuchs, Phys. Rev. Lett. **86**, 4267 (2001)
20. O. Glöckl, J. Heersink, N. Korolkova, G. Leuchs, S. Lorenz, J. Opt. B: Quant. Semiclass. Opt. **5**, S492 (2003)
21. J. Wenger, R. Tualle-Brouri, P. Grangier, Opt. Lett. **29**, 1267 (2004)
22. M.D. Reid, Phys. Rev. A **40**, 913 (1989)
23. D.F. Walls, G.J. Milburn, *Quantum Optics* (Springer, Berlin, 1994)
24. L.M. Duan, G. Giedke, J.I. Cirac, P. Zoller, Phys. Rev. Lett. **84**, 2722 (2000)
25. R. Simon, Phys. Rev. Lett. **84**, 2726 (2000)
26. V. Vedral, M.B. Plenio, M.A. Rippin, P.L. Knight, Phys. Rev. Lett. **78**, 2275 (1997)
27. J. Eisert, M.B. Plenio, Int. J. Quant. Inf. **1**, 479 (2003)
28. W.K. Wooters, Quant. Inf. Comput. **1**, 27 (2001)
29. G. Giedke, M.M. Wolf, O. Kruger, R.F. Werner, J.I. Cirac, Phys. Rev. Lett. **91**, 107901 (2003)
30. S.L. Braunstein, H.J. Kimble, Phys. Rev. A **61**, 042302 (2000)
31. T.C. Ralph, E.H. Huntington, Phys. Rev. A **66**, 042321 (2002)
32. A.M. Weiner, A.M. Kan'an, D.E. Leaird, Opt. Lett. **23**, 1441 (1998)
33. Y.Q. Li, D. Guzun, M. Xiao, Opt. Lett. **24**, 987 (1999)
34. R. Loudon, *Quantum Optics* (Springer, Berlin, 2000)
35. D.T. Smithey, M. Beck, M.G. Raymer, A. Faridani, Phys. Rev. Lett. **70**, 1244 (1993)
36. H. Hansen, T. Aichele, C. Hettich, P. Lodahl, A.I. Lvovsky, J. Mlynek, S. Schiller, Opt. Lett. **26**, 1430 (2001)